



Spatiotemporal Distribution Characterization for Terahertz Waves Generated From Plasma Induced by Two-Color Pulses

Erli Wang^{1,2}, Yulong Wang^{3,4}, Wenfeng Sun^{1,2*}, Xinke Wang^{1,2}, Shengfei Feng^{1,2}, Peng Han^{1,2}, Jiasheng Ye^{1,2} and Yan Zhang^{1,2}

¹Department of Physics, Capital Normal University, Beijing, China, ²Beijing Key Lab for Metamaterials and Devices, Key Laboratory of Terahertz Optoelectronics Ministry of Education, Beijing, China, ³Nanophotonics Research Center, Shenzhen Key Laboratory of Micro-Scale Optical Information Technology, Shenzhen University, Shenzhen, China, ⁴Songshan Lake Materials Laboratory, Dongguan, China

OPEN ACCESS

Edited by:

Yingxin Wang,
Tsinghua University, China

Reviewed by:

Jiayu Zhao,
University of Shanghai for Science and
Technology, China
Dong-Wen Zhang,
National University of Defense
Technology, China

*Correspondence:

Wenfeng Sun
wfsun@cnu.edu.cn

Specialty section:

This article was submitted to
Optics and Photonics,
a section of the journal
Frontiers in Physics

Received: 31 August 2021

Accepted: 20 September 2021

Published: 28 October 2021

Citation:

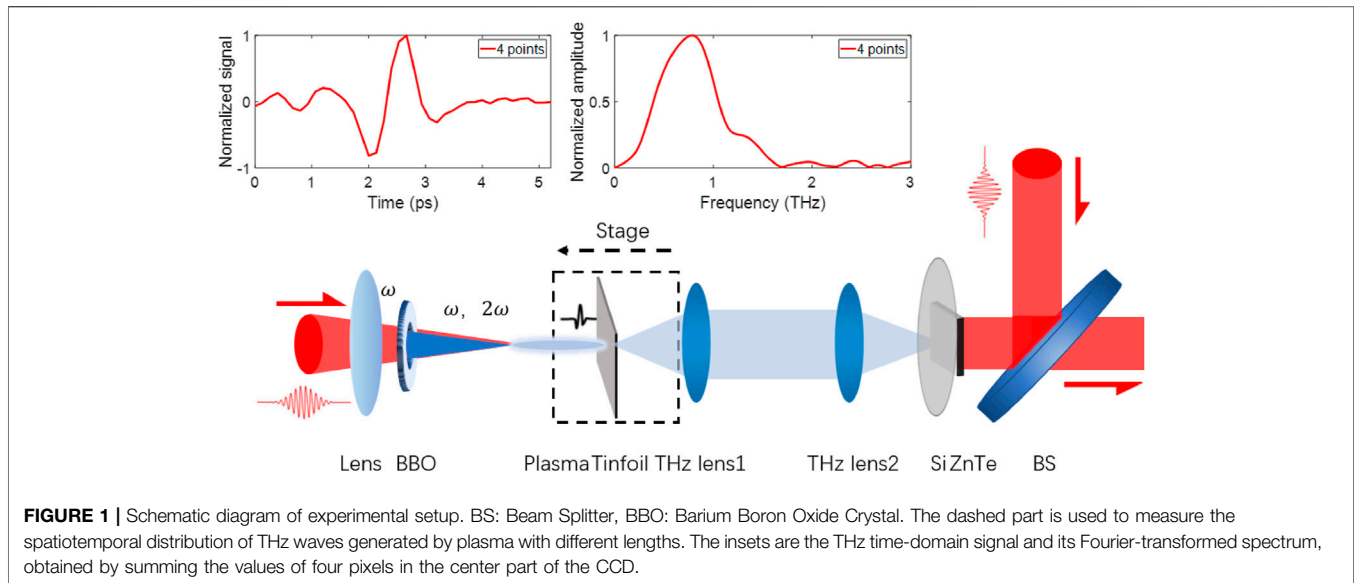
Wang E, Wang Y, Sun W, Wang X,
Feng S, Han P, Ye J and Zhang Y
(2021) Spatiotemporal Distribution
Characterization for Terahertz Waves
Generated From Plasma Induced by
Two-Color Pulses.
Front. Phys. 9:768186.
doi: 10.3389/fphy.2021.768186

The spatiotemporal distribution of terahertz (THz) radiation from plasma has been demonstrated with the technology of THz focal-plane imaging. It has been found that the spatiotemporal distribution will vary with the frequency, as well as the length of plasma. A doughnut-shaped distribution appears in the lower frequency range, while the bell-shaped distribution corresponds to the higher frequency range. For plasmas with different lengths, their generated THz images in the time domain are similar, the THz images in the frequency domain as well. The spatiotemporal distributions are simulated with the off-axis-phase matching theory. All the findings will renew the understanding of the THz generation from plasma induced by two-color pulses.

Keywords: THz focal plane imaging, plasma, off-axis-phase matching, spatiotemporal distribution, THz radiation

INTRODUCTION

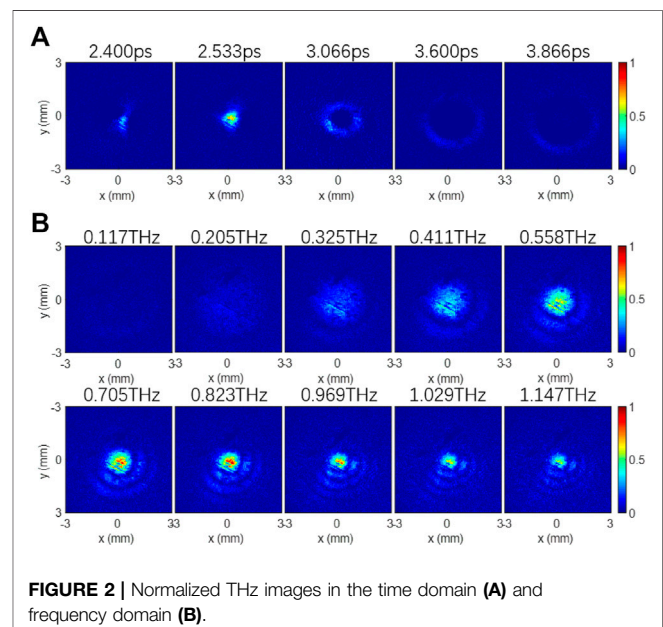
Terahertz (THz) wave generated from plasma has been proven to be a valuable tool in the field of nonlinear spectroscopy, imaging, and remote sensing [1–3]. The scheme of THz radiation from plasma induced by two-color laser pulses [4–7] has attracted more attention, and became popular owing to the emitted THz wave with broad spectrum and high intensity, as well as the good quality of polarization. With the widely application of THz radiation from two-color-induced plasma, its spatial characterization is desired. Many efforts have been put on this by using incoherent or coherent methods. The THz spatial distribution was deduced to be the shape of bell [8, 9] by raster scanning with the pyroelectric detectors or doughnut-shape [10] by raster scanning with Michelson interferometer; With a THz camera the transverse intensity of THz wave was captured and 3D-reconstructed to be the dumbbell shape [11]. There is also reported work contributing the conical hollow of THz distribution into the photo-induced carriers in the silicon wafer [12], which was used to filter the THz waves in the experiment. However, all these results seem incomplete for the comprehensive spatial characterization of THz waves. The influence of single-color plasma channel length on an angular THz radiation distribution was studied [13], yet its THz emission mechanism differs significantly from that of the two-color scheme. To fully understand the THz emission from two-color-induced plasma, it is necessary to characterize the spatiotemporal distribution of THz wave generated from plasma induced by two-color pulses.



In this work, the spatiotemporal distribution of THz wave radiated from plasma has been measured by using the technology of THz focal-plane imaging. For the plasma with unchanged length, THz spatial images in the time domain and frequency domain are presented, as well as their evolution. For plasmas with different lengths, the similarity and difference of the THz spatiotemporal distribution are also demonstrated. The experimental results are in accord with their simulations. These results are helpful in re-understanding the mechanism of the THz generation from plasma.

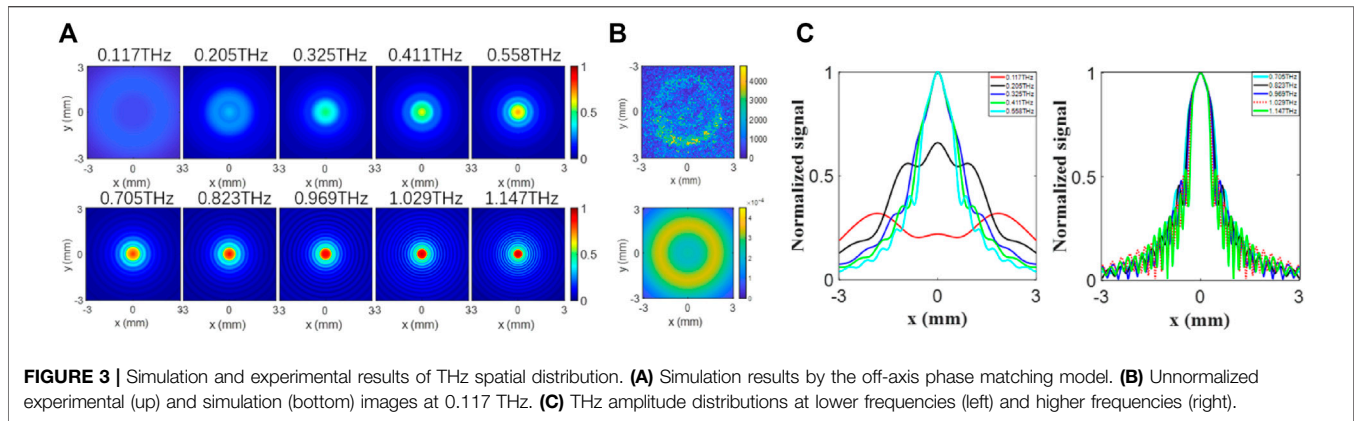
EXPERIMENTAL AND SIMULATION RESULTS

In the experiment, the technology of THz focal-plane imaging is used to obtain the spatiotemporal distribution of THz waves radiated from plasma induced by two-color pulses. The experimental setup is illustrated in **Figure 1**. A laser amplifier provides laser pulses with the central wavelength of 800 nm, repetition frequency of 1 kHz and pulse width of 35 fs. The femtosecond pulses are divided into two beams by a beam splitter (BS), one is used as the pump pulse and the other one is used as the probe pulse. The average pump and probe power are 700 and 13 mW, respectively. The pump pulse is focused by a lens with the focal length of 200 mm. With this lens, a relative uniform plasma about 7 mm is formed. There is a Barium Boron Oxide (BBO) crystal between the lens and its geometric focus. When the fundamental waves (800 nm) of femtosecond laser pass through the BBO crystal, their second harmonic waves generate. Both the fundamental (ω) and second harmonic (2ω) pulses ionize the air at the focus, which form a filament radiating THz waves. A 4f imaging system consisting of 2 THz lenses with the focal length of 100 mm and diameter of 75.8 mm is introduced in the THz beam. The front focal plane of the 4f imaging system coincides with the focus of the optical lens, while its back focal plane coincides with the ZnTe crystal ($<110>$, $10\text{ mm} \times 10\text{ mm} \times 1\text{ mm}$). With this 4f



imaging system, THz images delivered from the front focal plane to the detection crystal. A silicon wafer is used to combine the probe pulses and THz waves. The probe pulses are subjected to the refractive index modulation of the crystal by the THz electric field, then they are captured by a CCD. In the measurement, the images of THz waves have been extracted by the technology of dynamic matching and subtraction [14]. For clarity, the THz time-domain signal and its Fourier-transformed spectrum are also shown in the inset of **Figure 1**, which was obtained by summing the values of four pixels in the center part of the CCD.

In the experiment, by selecting proper experimental parameters, such like the crystal axis angle of the BBO crystal and the distance to the geometric focus of the focusing lens, the



generated THz signal was optimized. After that, the THz spatiotemporal distribution is measured and shown in **Figure 2A**. At the initial time of the THz pulse $t \leq 2.533$ ps, the spatial intensity distribution obtained by the above system is mainly concentrated near the center of the optical axis, like a solid bright spot. Thereafter, it diffuses when $t \geq 3.066$ ps, and the THz light spot diffuses into a hollow ring with the radius gradually increasing. In the process of diffusion, the amplitude of THz wave in the ring region decreases gradually due to the effect of divergence until the overall signal disappears. These THz temporal images were Fourier-transformed to obtain their field distributions at different frequencies. The results are shown in **Figure 2B**. For clearly, all images are normalized by the maximum value of the THz signal. It is clear that the THz field appears as a weak annular profile in the lower frequency range, while it appears in the region near the optical axis in the higher frequency range. With the frequency increasing, the annular side lobes gradually appear around the solid spot. Compared with that of the central spot the intensity of the annular side lobes becomes more and more obvious. It indicates that the radiation angle is corresponding to the frequency component of the radiated THz wave, which is consistent with the result reported in Ref. [15]. As illustrated in **Figure 2**, it seems that there are some nonuniform intensity distributions in these THz images, which was caused by some defects in the ZnTe crystal.

As shown in **Figure 2B**, with the frequency increasing, the spatial distribution of THz wave changes from the shape of doughnut to bell mixed with dark ring lobes. Currently, there are many theoretical models used to describe THz generation from ionized plasma, including the model of pondermotive, photocurrent, four-wave mixing and off-axis phase matching [7, 16–18]. Considering this experimental system, we adopt an off-axis phase matching model for simulation, in which the parameters similar to that in the experiment was selected. Different from the work in Ref. [16], the near-field profile of THz emission from the plasma has been calculated. For the case of plasma length shorter than the dephasing length, the near-field integration and their initial phases are also considered in the simulation. The simulation results are shown in **Figure 3A**. In the lower frequency range, $\nu \leq 0.558$ THz, the spatial distribution of

THz wave gradually changes from the shape of doughnut to bell, and the ring side lobes begin to appear; In the higher frequency range, $\nu \geq 0.705$ THz, the center spot of THz image becomes smaller and the annular side lobe becomes more obvious. According to the theory of off-axis phase matching, THz waves radiated from each point sources interfere constructively and accumulate continuously in the paraxial region; Away from the axis, THz waves interfere destructively and form alternative dark side ring lobes. For demonstration, we present the unnormalized experimental and simulated images at 0.117 THz, as shown in **Figure 3B**, the upper one is the experimental result, while the lower one is the simulated result. It is obviously that both the experimental and simulated spatial distributions are circular with the similar size, indicating that the theoretical simulation results are in good agreement with the experimental ones. To reveal the dependence of THz spatial distributions at different frequency, we extracted their THz amplitude information along the center line of the simulated images at different frequencies. The values of these curves were normalized by their own maximum, respectively, and plotted in **Figure 3C**. In **Figure 3C**, the left subfigure corresponds the lower frequency range $0.117 \text{ THz} \leq \nu \leq 0.558 \text{ THz}$, while the right one corresponds the higher frequency range $0.705 \text{ THz} \leq \nu \leq 1.147 \text{ THz}$. When $0.117 \text{ THz} \leq \nu \leq 0.325 \text{ THz}$, the simulated distribution transits gradually from the shape of annular to bell with the frequency increasing; When $\nu = 0.411$ THz, the ring side lobe appears. With the frequency increasing, the ring side lobe becomes more obvious, as shown in the right subfigure of **Figure 3C**. Comparing **Figure 3** with **Figure 2B**, one may find that more ring side lobes in the simulation results than that in the experimental ones, it may be caused by an error of optical focus position between the experiment and simulation.

In addition, images of THz radiation from plasma with different lengths are also obtained. As shown in the dashed part of **Figure 1**, a tinfoil is placed slightly away from the end of the plasma. Moving the tinfoil to make it approach the plasma end, until the tinfoil is penetrated by the plasma. Since the diameter of the hole on the tinfoil is similar to that of the plasma, we believe that the THz wave radiated from the plasma at the left side of the foil can be blocked and only the

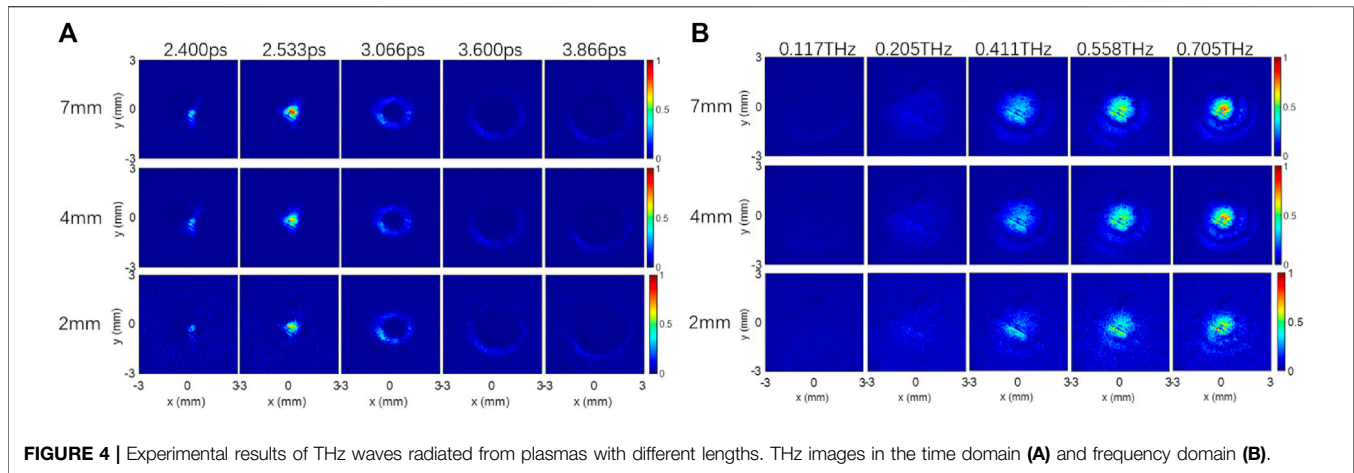


FIGURE 4 | Experimental results of THz waves radiated from plasmas with different lengths. THz images in the time domain (A) and frequency domain (B).

THz wave radiated from the plasma on the right side can be detected. By moving the foil to the left, the electric field E_i ($i = 1, 2, 3 \dots$) of THz waves radiated from plasma of different lengths can be obtained. For the case of plasma length comparable with the depth of field of the $4f$ system, the influence of the fixed front-focus of the $4f$ system on the experimental results is acceptable. In the experiment, we move the tinfoil across the plasma with the length of 7 mm by the step of 1 mm. The experimental results in the time domain and frequency domain are shown in **Figures 4A,B**, respectively. From **Figure 4A**, it can be found that the patterns of THz radiation from the plasmas with the same length diffuse from solid to hollow ring and then disappear over time. Moreover, the spatial shape and size of THz wave radiated from different lengths of plasma are maintained, but their intensities decrease with the plasma length shortened. Similarly, the images in **Figure 4A** are Fourier-transformed to obtain their frequency-domain images as shown in **Figure 4B**. For the plasmas of the same length, the spatial distribution of THz waves at different frequencies evolves from a doughnut-shape at low frequencies to a bell-shape at high frequencies; for the same frequency, the spatial distribution shape of THz waves radiated from different lengths of plasma is similar, while the intensity decreases with the decrease of plasma length. All these results indicate the accumulation effect of THz waves radiated from plasma.

It is known that the above THz electric fields E_i ($i = 1, 2, 3 \dots$) are generated from plasma fragments with different lengths, and these fragments are obtained by separating from one and the same filament. Thus, it allows us to achieve the THz electric fields at different positions of the plasma by subtracting the electric fields generated from the adjacent plasma fragments,

$$ME_{THzi} = E_i - E_{i-1} \quad (i = 1, 2, 3 \dots) \quad (1)$$

E_0 is the THz electric field when the plasma length is 0, i.e., $E_0 = 0$. It is reported that the peak frequency of the THz emission was used in characterizing the plasma density [19], the THz frequency corresponds to the plasma frequency, which can be written as,

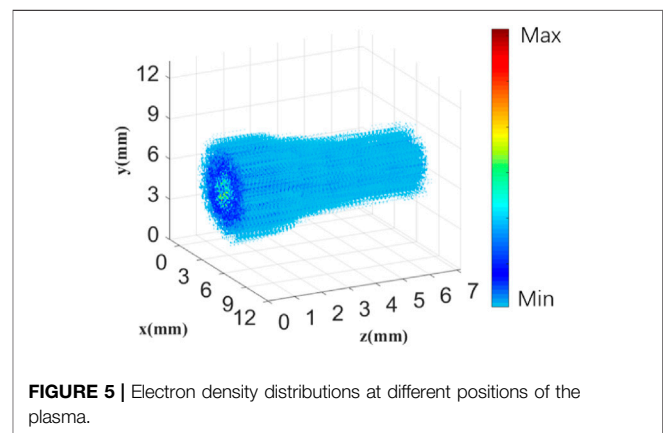


FIGURE 5 | Electron density distributions at different positions of the plasma.

$$\omega_p = \sqrt{4\pi e^2 n_e / m_e}, \quad (2)$$

Where n_e is the electron density and m_e is the electron mass. The electric field E_{THz} is proportional to the oscillation frequency of the plasma under the assumption of the appropriate laser field and gas density [20], meaning that $E_{THz} \propto \sqrt{n_e}$. Therefore, the electron density distributions at different positions of the plasma can be obtained, as shown in **Figure 5**. It can be found that the electron density of the plasma distributes symmetrically in the cross section. Additionally, the electron density is higher in the center of the plasma, and it decreases gradually with the increase of the diameter of the plasma. In the longitudinal direction, the electron density is also not uniform, and its density maximum locates near the beginning of the filament, which is in reasonable agreement with Refs. [19, 21–23].

CONCLUSION

The THz spatiotemporal distribution of THz radiation from plasma has been measured by the technology of THz focal-plane imaging. With the off-axis phase matching model, we obtained their simulation results, and the simulation results are in good agreement with the experimental ones. THz spatial distributions are doughnut-shape at low frequencies and bell-shape at high frequencies. The spatiotemporal distribution characteristics of THz wave from

plasmas with different lengths are similar, but their intensities depend on the length of the plasma seriously. With the THz images radiated from plasmas of different lengths, the electric density inside of the plasma has been revealed.

DATA AVAILABILITY STATEMENT

The original contributions presented in the study are included in the article/Supplementary Material, further inquiries can be directed to the corresponding author.

AUTHOR CONTRIBUTIONS

EW, YW, and WS contributed to experiment and simulation. WS designed the study. XW, SF, PH, JY, and YZ performed the

theoretical analysis. All authors contributed to article revision, read, and approved the submitted version.

FUNDING

The National Natural Science Foundation of China (61735002, 11774243, 11774246, 11474206, 11404224); Youth Innovative Re-search Team of Capital Normal University (19530050146, 18530500155, 20530290053); Connotative Development Foundation for Distinguished Young Talents in Capital Normal University (2055105); Capacity Building for Science and Technology Innovation-Fundamental Scientific Research Funds (20530290072, 19530050170, 19530050180, 18530500186, 025185305000/142, 025185305000/142).

REFERENCE

- Kampfrath T, Sell A, Klatt G, Pashkin A, Mährlein S, and Dekorsy T. Coherent Terahertz Control of Antiferromagnetic Spin Waves. *Nat Photon* (2011) 5: 31–4. doi:10.1038/nphoton.2010.259
- Ulbricht R, Hendry E, Shan J, Heinz TF, and Bonn M. Carrier Dynamics in Semiconductors Studied with Time-Resolved Terahertz Spectroscopy. *Rev Mod Phys* (2011) 83:543–86. doi:10.1103/revmodphys.83.543
- Liu J, Dai J, Chin SL, and Zhang X-C. Broadband Terahertz Wave Remote Sensing Using Coherent Manipulation of Fluorescence from Asymmetrically Ionized Gases. *Nat Photon* (2010) 4:627–31. doi:10.1038/nphoton.2010.165
- Zhang XC, Shkurinov A, and Zhang Y. Extreme Terahertz Science. *Nat Photon* (2017) 11:16–8. doi:10.1038/nphoton.2016.249
- Clerici M, Peccianti M, Schmidt BE, Caspani L, Shalaby M, and Giguère M. Wavelength Scaling of Terahertz Generation by Gas Ionization. *Phys Rev Lett* (2013) 110:253901. doi:10.1103/physrevlett.110.253901
- Siegel PH. Terahertz Technology in Biology and Medicine. *IEEE Trans Microwave Theor Techn*. (2004) 52(10):2438–47. doi:10.1109/tmtt.2004.835916
- Cook DJ, and Hochstrasser RM. Intense Terahertz Pulses by Four-Wave Rectification in Air. *Opt Lett* (2000) 25(16):1210–2. doi:10.1364/ol.25.001210
- Akhmedzhanov RA, Ilyakov IE, Mironov VA, Suvorov EV, Fadeev DA, and Shishkin BV. Generation of Terahertz Radiation by the Optical Breakdown Induced by a Bichromatic Laser Pulse. *J Exp Theor Phys* (2009) 109(3):370–8. doi:10.1134/s1063776109090027
- Zhong H, Karpowicz N, and Zhang X-C. Terahertz Emission Profile from Laser-Induced Air Plasma. *Appl Phys Lett* (2006) 88(26):261103. doi:10.1063/1.2216025
- Andreeva VA, Kosareva OG, Panov NA, Shipilo DE, Solyankin PM, and Esaulkov MN. Ultrabroad Terahertz Spectrum Generation from an Air-Based Filament Plasma. *Phys Rev Lett* (2016) 116(6):063902–5. doi:10.1103/physrevlett.116.063902
- Klarskov P, Strikwerda AC, Iwaszczyk K, and Jepsen PU. Experimental Three-Dimensional Beam Profiling and Modeling of a Terahertz Beam Generated from a Two-Color Air Plasma. *New J Phys* (2013) 15(7):075012–3. doi:10.1088/1367-2630/15/7/075012
- Sørensen C, Guiramand L, Deger J, Tondusson M, Skovsen E, and Freysz E. Conical versus Gaussian Terahertz Emission from Two-Color Laser-Induced Air Plasma Filaments. *Opt Lett* (2020) 7(45):2132–5. doi:10.1364/OL.390112
- Koribut AV, Rizaev GE, Mokrousova DV, Savinov SA, Reutov AA, and Mityagin YA. Similarity of Angular Distribution for THz Radiation Emitted by Laser Filament Plasma Channels of Different Lengths. *Opt Lett* (2020) 45(45):4009–11. doi:10.1364/OL.394377
- Wang X, Cui Y, Sun W, Ye J, and Zhang Y. Terahertz Real-Time Imaging with Balanced Electro-Optic Detection. *Opt Commun* (2010) 283(23):4626–32. doi:10.1016/j.optcom.2010.07.010
- Zhao J, Chu W, Wang Z, Peng Y, Gong C, and Lin L. Strong Spatial Confinement of Terahertz Wave inside Femtosecond Laser Filament. *ACS Photon* (2016) 3(12):2338–43. doi:10.1021/acsp Photonics.6b00512
- You YS, Oh TI, and Kim KY. Off-axis Phase-Matched Terahertz Emission from Two-Color Laser-Induced Plasma Filaments. *Phys Rev Lett* (2012) 109(18):183902–5. doi:10.1103/physrevlett.109.183902
- Borodin AV, Panov NA, Kosareva OG, Andreeva VA, Esaulkov MN, and Makarov VA. Transformation of Terahertz Spectra Emitted from Dual-Frequency Femtosecond Pulse Interaction in Gases. *Opt Lett* (2013) 38(38): 1906–8. doi:10.1364/OL.38.001906
- Béjot P, Kasparian J, and Wolf J-P. Dual-color Co-filamentation in Argon. *Opt Express* (2008) 16(18):14115–27. doi:10.1364/oe.16.014115
- Wang T-J, Ju J, Wei Y, Li R, Xu Z, and Chin SL. Longitudinally Resolved Measurement of Plasma Density along Femtosecond Laser Filament via Terahertz Spectroscopy. *Appl Phys Lett* (2014) 105:051101. doi:10.1063/1.4892424
- Kim K-Y, Glowina JH, Taylor AJ, and Rodriguez G. Terahertz Emission from Ultrafast Ionizing Air in Symmetry-Broken Laser fields. *Opt Express* (2007) 15(8):4577–84. doi:10.1364/oe.15.004577
- Gaarde MB, and Couairon A. Intensity Spikes in Laser Filamentation: Diagnostics and Application. *Phys Rev Lett* (2009) 103:043901. doi:10.1103/PhysRevLett.103.043901
- Chen Y, Théberge F, Kosareva O, Panov N, Kandidov VP, and Chin SL. Evolution and Termination of a Femtosecond Laser Filament in Air. *Opt Lett* (2007) 32(24):3477–9. doi:10.1364/ol.32.003477
- Sun X, Xu S, Zhao J, Liu W, Cheng Y, and Xu Z. Impressive Laser Intensity Increase at the Trailing Stage of Femtosecond Laser Filamentation in Air. *Opt Express* (2012) 20(4):4790–5. doi:10.1364/oe.20.004790

Conflict of Interest: The authors declare that the research was conducted in the absence of any commercial or financial relationships that could be construed as a potential conflict of interest.

Publisher's Note: All claims expressed in this article are solely those of the authors and do not necessarily represent those of their affiliated organizations, or those of the publisher, the editors and the reviewers. Any product that may be evaluated in this article, or claim that may be made by its manufacturer, is not guaranteed or endorsed by the publisher.

Copyright © 2021 Wang, Wang, Sun, Wang, Feng, Han, Ye and Zhang. This is an open-access article distributed under the terms of the Creative Commons Attribution License (CC BY). The use, distribution or reproduction in other forums is permitted, provided the original author(s) and the copyright owner(s) are credited and that the original publication in this journal is cited, in accordance with accepted academic practice. No use, distribution or reproduction is permitted which does not comply with these terms.